Transonic Region of High Dynamic Response Encountered on an Elastic Supercritical Wing

David A. Seidel,* Clinton V. Eckstrom,† and Maynard C. Sandford†
NASA Langley Research Center, Hampton, Virginia

Unsteady aerodynamic data were measured on a 10.3 aspect-ratio elastic supercritical wing while undergoing high dynamic response above a Mach number of 0.90. These tests were conducted in the NASA Langley Transonic Dynamics Tunnel. A previous test of this wing predicted an unusual instability boundary based upon subcritical response data. During the present test, no instability was found, but an angle-of-attack dependent narrow Mach number region of high dynamic wing response was observed over a wide range of dynamic pressures. The effect on dynamic wing response of wing angle of attack, static outboard control surface deflection and a lower surface spanwise fence located near the 60% local chordline was investigated. The driving mechanism of the dynamic wing response appears to be related to chordwise shock movement in conjunction with flow separation and reattachment on both the upper and lower surfaces.

Nomenclature

C_L = lift coefficient
C_p = pressure coefficient
h = altitude, ft
M = freestream Mach number
q = freestream dynamic pressure, psf
R = Reynolds number, ft^{-1}
x/c = fraction of local chord
α = wing root angle of attack, deg (positive leading-edge up)
δ_m = mean control surface deflection angle, deg (positive trailing-edge down)
ΔC_p = lifting pressure coefficient (positive up)
η = fraction of semispan

Introduction

SINGLE degree-of-freedom bending mode oscillations have unexpectedly been encountered during experiments with several aircraft configurations. These oscillations are characteristically large-amplitude oscillations in a low-frequency vibration mode and tend to be angle-of-attack dependent. These oscillations have been observed on a low-aspect-ratio wing with subsonic airfoil shape,[1] on the B-1A during a wind-up turn,[2] on the canard of the HIMAT aeroelastic model at negative angle of attack,[2] and on a forward-swept wing force model wing panel at a negative angle of attack.[2] Linear-theory flutter analysis was unable to predict any of these oscillations. The B-1 instability has been attributed to a dynamic leading-edge vortex flow mechanism. The other instabilities are attributed to transonic shock-wave motion coupling with the first wing bending mode.

An unusual transonic instability also was encountered near $M=0.9$ during an unsteady pressure test of the second Aeroelastic Research Wing (ARW-2)[3] of the NASA Drones for Aerodynamic and Structural Testing (DAST) program.[3,4] This aeroelastic supercritical wing was initially tested in October 1983 in the NASA Langley Transonic Dynamics Tunnel (TDT). The wing had an aspect ratio of 10.3 and a leading-edge sweepback angle of 28.8 deg. The wing also had a hydraulically driven outboard trailing-edge control surface and was instrumented with dynamic pressure transducers. This unusual transonic instability boundary was predicted using a subcritical response technique. This instability was predicted to occur at an almost constant Mach number of 0.9 for all dynamic pressures tested. The wing motion was primarily first wing bending-mode response and was angle-of-attack dependent. Identifying such an unusual transonic instability boundary appears to be beyond the scope of linear-theory analysis.[4]

Thus, a second wind-tunnel test was performed on the DAST ARW-2 wing to further investigate this unusual instability. The primary purpose of the test was to establish firmly the existence of the instability boundary and to gather wing-response data and dynamic pressure measurements to help understand the mechanism forcing the wing oscillations.

This paper presents the results from this second wind-tunnel test of the DAST ARW-2 wing. Dynamic wing motion and pressures were measured for wind-tunnel Mach numbers from 0.50–0.96 at dynamic pressures from 100 to over 340 psf. Wool tufts were used to visualize the flow patterns on the wing in the instability region. The effects on dynamic wing response of wing angle of attack, static outboard control surface deflection, and a spanwise fence on the lower surface were investigated.

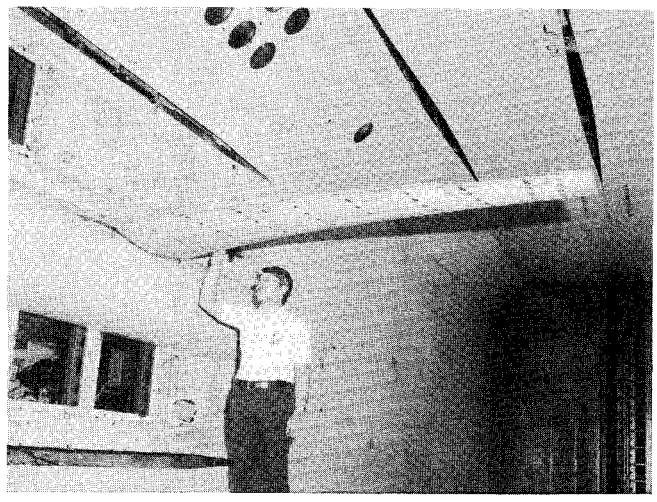

Fig. 1 Wing mounted in TDT test section.

Presented as Paper 87-0735 at the AIAA/ASME/ASCE/AHS 28th Structures, Structural Dynamics, and Materials Conference, Monterey, CA, April 6–8, 1987; received March 31, 1987; revision received Feb. 19, 1988.

*Aerospace Engineer, Unsteady Aerodynamics Branch, Structural Dynamics Division. Member AIAA.

†Aerospace Engineer, Configuration Aeroelasticity Branch, Structural Dynamics Division. Member AIAA.

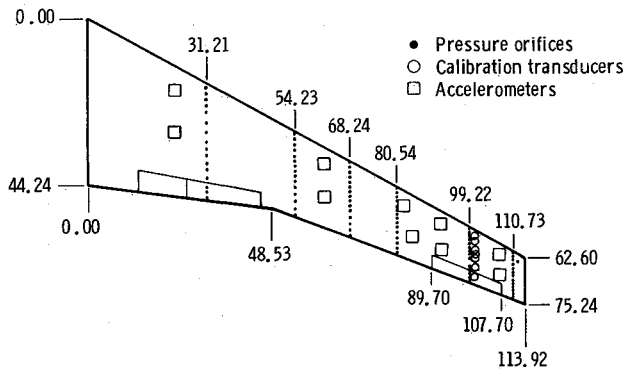

Fig. 2 Wing planform and instrumentation locations, in.

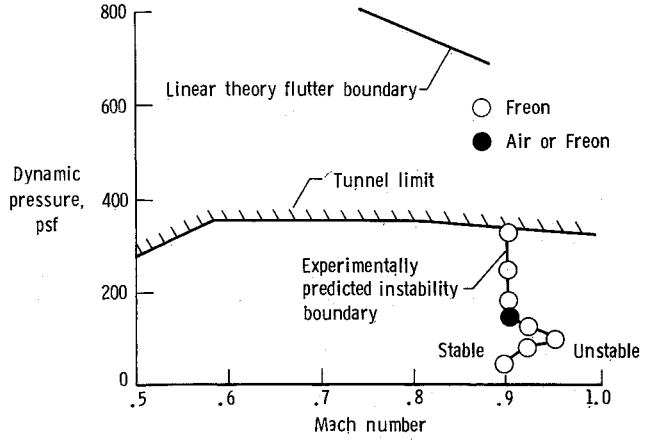

Fig. 3 Experimental and linear-theory predictions of wing instability boundary.

Model

Figure 1 shows the wing and fuselage configuration mounted in the wind tunnel. The elastic semispan wing used in the present study is the DAST ARW-2 right wing panel. A half-body fuselage was used to simulate the drone fuselage. This fuselage had shorter nose and tail sections than does the drone fuselage since no supersonic tests were to be made. The center section of the fuselage was similar to the actual drone fuselage in both diameter and wing location to generate the proper airflow over the inboard section of the wing. Both the fuselage and the wing were mounted on a remotely controlled turntable mechanism located on the tunnel sidewall.

The wing planform is shown in Fig. 2. The wing had an aspect ratio of 10.3 with a leading-edge sweep angle of 28.8 deg. The wing was equipped with three hydraulically driven control surfaces, two inboard and one outboard. For this test, the inboard surfaces were held fixed at 0-deg deflection and only the outboard surface was deflected statically. The outboard surface hinge line was located at 77% of local chord.

The wing contour was formed from three different supercritical airfoils as described in Ref. 5. These three airfoils were located at the following spanwise wing stations: the wing-fuselage junction ($\eta = 0.071$), the wing planform break ($\eta = 0.426$), and the wing tip ($\eta = 1.000$), and had thickness-to-chord ratios of 0.146, 0.120, and 0.106, respectively. The three supercritical airfoil shapes and wing twist were defined for the design cruise condition and are described in Ref. 6. The wing-design shape was defined by using straight-line interpolation along constant percent chords between these three airfoil sections for the design cruise conditions of $M = 0.80$, $C_L = 0.53$ ($\alpha = 1.3$ deg), and $h = 46{,}800$ ft ($q = 127$ psf). The jig shape for fabrication of the flexible wing was determined by first calculating the wing load distribution at the design cruise conditions. The second step was to calculate the wing deflection and twist for the wing-load distribution using a finite-element structural model of the wing. The final step was to subtract the calculated wing deflection and twist from the wing-design shape to define the wing-jig shape.

The wing primary structure consisted of a front spar at 25% of local chord and a rear spar at 62% of local chord.[6] Ribs were placed perpendicular to the rear spar every 13.2 in. except for the outboard wing-tip rib, which also served as a spar-end fitting. The spars and ribs were machined from 7075-T73 aluminum alloy. The wing skin was made of fiberglass material with honeycomb panels sandwiched between the middle two layers of fiberglass for areas of skin not located over the spars or ribs. The number of layers of fiberglass used to make the skin varied from 36 at the inboard end to 27 at the outboard end with approximately 25% of the layers at ±45 deg orientation.

Also shown in Fig. 2 are the locations of the wing instrumentation. The instrumentation consisted of 191 dynamic pressure transducers and 10 accelerometers. In addition, strain gage bridges were located near the wing root to measure bending moments. Differential pressure gages were mounted in each supply line to the hydraulic actuators of each control surface to measure hinge moments. Small potentiometers were used to measure the control surface angular displacement. The model angle of attack was measured by a servo accelerometer that was mounted near the wing root. Both steady and unsteady pressures were obtained using differential pressure transducers referenced to the tunnel's static pressure. Streamwise rows of upper and lower surface pressure orifices were located at six span stations: $\eta = 0.274$, 0.476, 0.599, 0.707, 0.871, and 0.972. The fifth row at $\eta = 0.871$ lies along the midspan of the outboard control surface. All of these surface orifices were connected to pressure transducers by matched tubes having an inner diameter of 0.040 in. and a length of 18 in. In order to determine the tube transfer functions needed to correct the unsteady pressure data from these matched-tube transducers, simultaneous measurements were also obtained from a row of in-situ transducers mounted on the wing upper surface at $\eta = 0.875$, parallel to the fifth row of surface orifices. Dynamic wing deflections were determined using the 10 accelerometers.

Wind Tunnel

The NASA Langley Transonic Dynamics Tunnel is a closed-circuit, continuous-flow tunnel that has a 16-ft-square test section with slots in all four walls. Mach number and dynamic pressure can be varied simultaneously, or independently, with either air or Freon as a test medium. Freon was used for the tests in this investigation.

Data Acquisition and Analysis

Data from the model instrumentation were acquired using the TDT real-time data acquisition system.[7] The pressure data were acquired using the electronically scanned pressure (ESP) system.[8] The ESP system is a sequential, digital-pressure sampling system equivalent to a mechanical Scanivalve. All of the data were digitized in real-time and written on magnetic tape for later analysis. The three inboard rows of surface orifices were digitized at 31.25 samples/s while the three outboard rows were digitized at 250 samples/s. All other data, including model and tunnel conditions and wing accelerometers, were digitized at 1000 samples/s.

Static pressures were recorded for all six rows of surface orifices. Each pressure signal was averaged for 300 samples to acquire its mean value. Wing bending moments were measured for all cases where static pressures were recorded. The bending-moment measurements were averaged for 0.3 s to obtain a mean value. Dynamic time histories were recorded for the three outboard rows of surface orifices and all 10 wing accelerometers. The dynamic time histories were recorded for a minimum of 15 s at each flow condition.

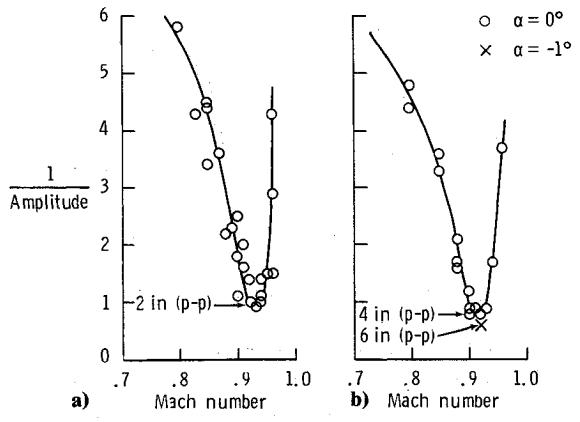

Fig. 4 Peak-hold response data from wing-tip accelerometer at $\delta_m = 0$ deg: a) $q = 125$–166 psf; and b) $q = 260$–340 psf.

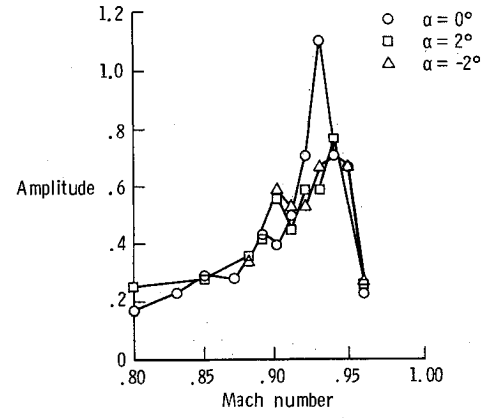

Fig. 5 Peak-hold response data from wing-tip accelerometer for three angles of attack at $\delta_m = 0$ deg and $q = 125$–166 psf.

Previous Test Results

During the first test of the ARW-2 wing in the TDT, an unusual wing instability, with motion similar to the wing first bending mode, was encountered.[4] The boundary was determined for a wing angle of attack and control surface deflection of 0 deg within the wind-tunnel limits as shown in Fig. 3. Also shown in Fig. 3 as a solid line is the predicted linear-theory (doublet lattice theory) flutter boundary, which is of a conventional nature, exhibiting a drop in the dynamic pressure at flutter as Mach number increases. Typically, experimental flutter boundaries attain a minimum value of dynamic pressure near $M \approx 1.0$ followed by a rapid rise in the flutter dynamic pressures as speed increases further. This is in contrast with the experimental instability boundary shown in Fig. 3, which is nearly vertical at a Mach number of 0.90. The measured boundary was determined using a familiar subcritical response technique known as peakhold.[9] The peakhold results definitely showed indication of instability onset. However, the normal verification procedure of obtaining hard instability (zero damping) points was avoided for fear of damaging the model which was to be used in future flight programs. The boundary was predicted to occur at a nearly constant Mach number of 0.90 beginning at a low dynamic pressure of about 50 psf ($R = 874{,}000$) and rising nearly vertical to over 300 psf ($R = 5{,}300{,}000$). The observed wing motion during the instability was similar to the wing first bending mode, the frequency of which was measured to be 8.3 Hz in the wind-off vibration tests. The instability frequency was 8.6 Hz at the lowest dynamic pressure point and increased with dynamic pressure to about 13 Hz at the highest dynamic pressure point. It is interesting to note that the predicted flutter frequency (using doublet lattice linear-theory aerodynamics) was 24.3 Hz at a Mach number of 0.80. An attempt to predict the instability using a three-dimensional transonic small-disturbance code was unsuccessful as described in Ref. 10.

Because of recent interest in angle-of-attack effects and shock-induced effects on wing instabilities,[11] several additional test runs were made. These runs included variation of the wing angle of attack as the predicted instability boundary was approached, comparison using air or Freon as the test medium, and comparison with and without a transition strip near the wing leading edge. The instability was found to be sensitive to variation in angle of attack and, generally, the minimum damping occurred at or near zero wing-root angle of attack. In Fig. 3, the solid symbol indicates the Mach number and dynamic pressure where the comparison tests were made. The results showed no significant difference in the instability boundary for tests in air or Freon. Reynolds number values in Freon are approximately 3.1 times greater than those obtained in air. There were also no significant differences for tests in Freon with or without a transition strip.

Present Test Results and Discussion

Dynamic pressures and wing deflections were measured for a large number of test conditions in the TDT using Freon as a test medium. Data were taken at Mach numbers from 0.5–0.96 for two stagnation pressures. For a Mach number range of 0.8–0.96, the two stagnation pressures gave a dynamic pressure variation of 125–166 psf and 260–340 psf. These two stagnation pressures will be referred to as the low- and high-density conditions.

Dynamic Wing Response

Dynamic wing-response variations as a function of Mach number are presented to examine the effects of changing density conditions and model angle of attack. Also, the effects of static outboard control surface deflection and the addition of a spanwise fence on the lower surface are examined. All dynamic wing-response data presented are obtained from the rear wing-tip accelerometer.

Mach Number and Dynamic Pressure Effects

Figure 4 shows the peak-hold results from the wing-tip accelerometer for both the low- and high-density conditions. The wing angle of attack and control surface deflection were held at 0 deg. The data show that no instability was found but instead a region of high dynamic wing response was observed. For the lower density condition ($q = 125$–166 psf), the wing motion reaches a maximum at $M = 0.93$ and then rapidly decreases with increasing Mach number. The same trend occurs for the higher density condition ($q = 260$–340 psf) with maximum wing motion occurring near $M = 0.92$. The observed wing-tip maximum dynamic amplitudes are noted in Fig. 4. At the lower density condition, the amplitude of the wing-tip motion was approximately 2 in. peak-to-peak. At the higher density condition, which has double the dynamic pressure, the amplitude of the wing-tip motion doubled to approximately 4 in. peak-to-peak.

Also shown in Fig. 4b at $M = 0.92$ is a single point for $\alpha = -1$ deg, where 6 in. peak-to-peak amplitude of wing-tip motion was observed. At this condition, the wing motion was so severe that the tunnel bypass valves were opened to rapidly reduce the dynamic pressure and associated wing motion.

Angle-of-Attack Effects

Figure 5 shows the peak-hold results from the wing-tip accelerometer for three wing angles of attack at the lower density condition. The mean control surface deflection was held at 0 deg. As shown in the figure, the maximum dynamic wing response occurred for a wing angle of attack of 0 deg at $M = 0.93$. Changing the wing angle of attack to 2 and -2 deg decreased the maximum wing response and shifted the corresponding Mach number to 0.94. Similar angle-of-attack trend

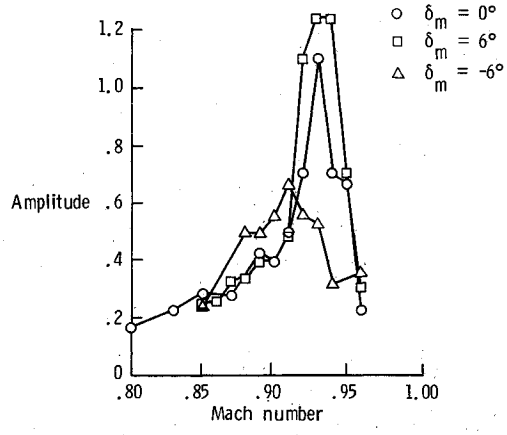

Fig. 6 Peak-hold response data from wing-tip accelerometer for three mean control surface deflection angles at $\alpha = 0$ deg and $q = 125$–166 psf.

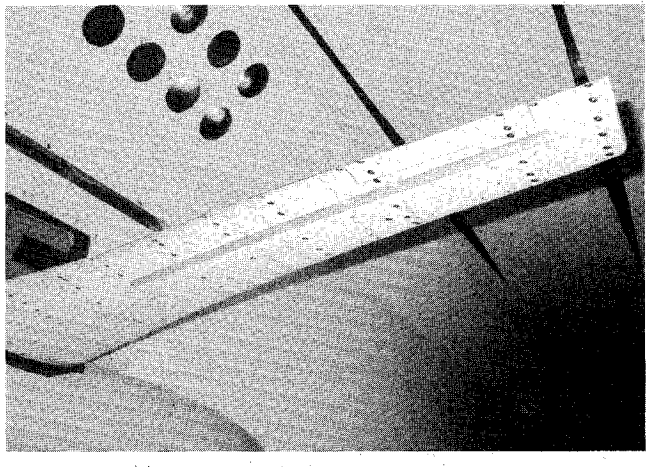

Fig. 7 Wing with spanwise fence attached to lower surface.

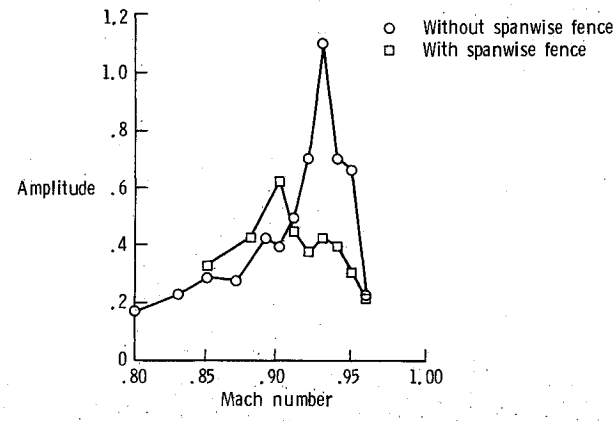

Fig. 8 Peak-hold response data from wing-tip accelerometer for wing with and without lower surface spanwise fence at $\alpha = 0$ deg, $\delta_m = 0$ deg, and $q = 125$–166 psf.

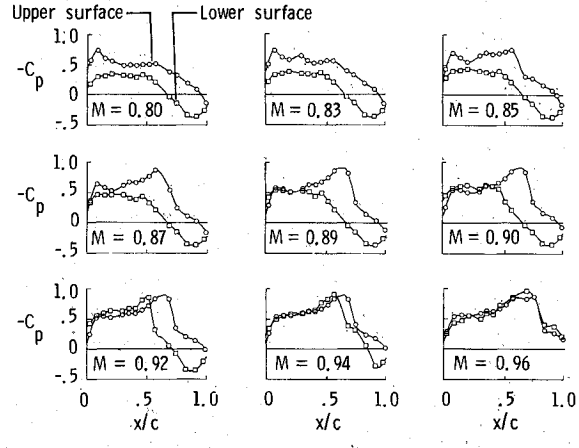

Fig. 9 Mean chordwise pressure distributions for nine Mach numbers at $\eta = 0.871$, $\alpha = 0$ deg, $\delta_m = 0$ deg, and $q = 125$–166 psf.

results were seen at the higher density condition. Data were taken for wing angles of attack of 1, 0, and −1 deg up to $M = 0.9$ and fell within the scatter of the experimental data observed at 0 deg as shown in Fig. 4. Therefore, it is believed that for this configuration the maximum wing response occurs when the wing angle of attack is nominally at 0 deg.

Control Surface Effects

Figure 6 shows the peak-hold results from the wing-tip accelerometer for three outboard control surface mean deflection angles at the lower density condition. The wing angle of attack was set at 0 deg. The figure shows a small increase in wing response for the control surface deflection of 6 deg (trailing-edge down). However, a significant reduction in wing response is shown for a deflection of −6 deg. The wing-tip maximum response peak is reduced by half and shifted to a lower Mach number of 0.91.

Lower Surface Spanwise Fence Effects

In an attempt to disturb the flow and change the dynamic wing response, a 1/2-in. high spanwise fence was attached to the lower surface at approximately the 60% local chordline as shown in Fig. 7. The fence ran from the wing planform break ($\eta = 0.426$) to within 5 in. of the wing tip ($\eta = 0.956$). The fence was made up of five separate 1-ft-long pieces of aluminum placed end to end to minimize increasing the wing stiffness. The effect of the fence on the wing-tip accelerometer peak-hold response at the lower density condition is shown in Fig. 8. The fence has a significant effect upon the wing response, lowering the amplitude of maximum wing motion and shifting the peak value to a lower Mach number of 0.90.

Mean Pressures

Figure 9 shows the mean chordwise pressure distribution at the 87.1% span station for nine Mach numbers at the lower density condition. The wing angle of attack and outboard mean control surface deflection were 0 deg. As Mach number increases, a shock develops on the upper surface at $M = 0.85$ and becomes quite strong at $M = 0.89$. The criteria used to determine trailing-edge flow separation from mean pressure measurements is the attainment of negative pressure coefficients at the 95% chord location. When negative pressures are sustained aft of this location, the flow is considered to be separated. Based upon the mean pressure distributions shown in Fig. 9, it appears that flow separation on the upper surface is evident at $M = 0.92$ and is established strongly at $M = 0.94$. The lower surface develops a strong shock at $M = 0.92$, and the pressure distributions indicate flow separation at $M = 0.96$.

Flow Visualization

Wool tufts were placed on the upper and lower wing surfaces for several test runs to visualize the flow patterns on the wing. The tufts were placed on eight span stations located at $\eta = 0.517$, 0.558, 0.635, 0.671, 0.761, 0.816, 0.905, and 0.938, as shown in Fig. 10. The tufts were 1 in. long and on the six inboard span stations were located at every 10% of local chord. On the two outboard span stations, the tufts were located between 10 and 90% chord at every 20% of local chord.

Table 1 lists the regions of separated flow on the wing as indicated by the tuft data for Mach numbers from 0.85–0.96 at the lower density condition. Upper surface flow separation is first indicated at $M = 0.88$. The region of separated flow expands upstream and outboard as Mach number increases to

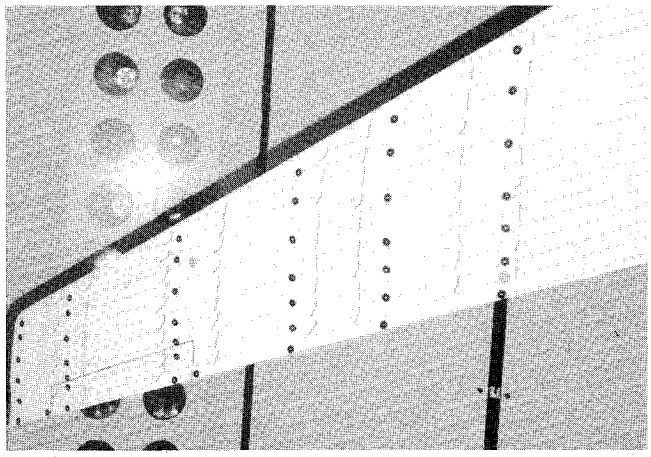

Fig. 10 Wool tufts installed on wing lower surface.

Table 1 Separated flow regions as shown by wool tufts

	Region of separated flow			
	Upper surface		Lower surface	
M	x/c	η	x/c	η
0.85	—	—	—	—
0.88	0.8–1.0	0.517–0.816	—	—
0.90	0.7–1.0	0.517–0.905	0.6–1.0	0.635–0.761
0.92	0.7–1.0	0.517–0.938	0.6–1.0	0.635–0.938
0.94	0.6–1.0	0.517–0.938	0.5–1.0	0.635–0.938
0.96	0.6–1.0	0.517–0.938	0.6–1.0	0.635–0.905

0.94 and then remains constant to $M=0.96$. Flow separation on the lower surface is initially indicated at $M=0.90$. The region of separated flow expands upstream and outboard as Mach number increases to 0.94. At $M=0.96$, the region of separated flow on the lower surface decreases, moving downstream and inboard.

Comparing this data to the mean pressure distributions shown in Fig. 9 leads to two conclusions. The first is that the mean pressure data gives an incomplete picture of the flow separation. The mean pressure data, taken at $\eta=0.871$, does not indicate flow separation on the upper surface until $M=0.92$, whereas the wool tufts indicate separation in the region of the pressure transducers near $M=0.89$. Flow separation on the lower surface is not indicated by the mean pressures until $M=0.96$, whereas the tufts indicate separation in the region at $M=0.92$. The second conclusion is that flow separation, as shown by the tuft data, coincides with the occurrence of strong shocks on a surface, as shown by the mean pressure data in Fig. 9. This flow separation occurs near $M=0.89$ on the upper surface and $M=0.92$ on the lower surface at the 87.1% span station.

Wing Deflection and Twist

During the test, measurements of the mean wing-tip deflection and twist were made using an optical cathetometer instrument focused on a straight line drawn on the outboard tip of the wing. The results of the wing-tip measurements for the lower density condition at a wing angle of attack and mean control surface deflection of 0 deg are shown in Fig. 11. The wing-tip deflection and twist increase as Mach number increases up to a maximum near $M=0.85$. At higher Mach numbers, the wing-tip deflection and twist values decrease rapidly as the Mach number increases. This agrees with the tuft data which shows flow separation beginning on the upper surface at $M=0.88$, causing loss of lift (see Fig. 9) and the resulting decrease in wing deflection and twist.

Instantaneous Pressures

Figure 12 shows the instantaneous chordwise pressure distribution at the 87.1% span station for $M=0.92$, $\alpha=1$ deg, and

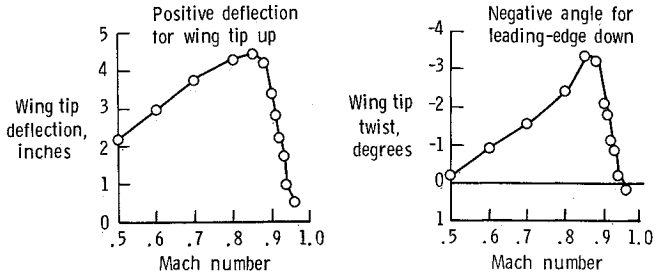

Fig. 11 Measured mean wing-tip deflection and twist vs Mach number at $\alpha=0$ deg, $\delta_m=0$ deg, and $q=100$–166 psf.

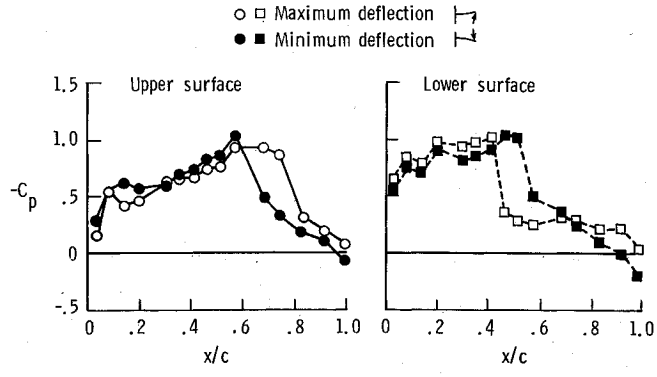

Fig. 12 Instantaneous chordwise pressure distributions at maximum and minimum wing-tip deflection at $\eta=0.871$, $M=0.92$, $\alpha=-1$ deg, and $\delta_m=0$ deg.

$\delta_m=0$ deg. This is the condition at which 6-in. peak-to-peak wing-tip motion occurred (Fig. 4b). The instantaneous pressure distributions are shown for the maximum and minimum vertical wing-tip deflection. Based upon the pressure at 95% chord, at the maximum wing-tip deflection the flow aft of the shock is separated on the upper and lower surfaces. The flow is attached on both surfaces when the vertical tip deflection is a minimum.

This figure points out an important feature of this dynamic motion. At conditions where large-amplitude dynamic motion is encountered, the trailing-edge flow begins a pattern of separating and reattaching on the wing, which coincides with the shock-wave motion. As the Mach number is increased above 0.92, the flow behind the shock remains separated (see Fig. 9) and the amplitude of the motion rapidly decreases (see Fig. 4). Thus, it appears that the dynamic wing response is related to chordwise shock motion in conjunction with shock-induced flow separation and reattachment on both the upper and lower surfaces. This conclusion is supported further by the results obtained when the spanwise fence was attached to the wing lower surface. The fence prevented reattachment of the flow on that surface and the maximum wing motion was found to be dramatically reduced, as shown in Fig. 8.

The alternating separation and reattachment of the flow on the upper and lower surfaces also explains the discrepancy between the mean pressure and wool tuft data. The mean pressure data gives an average of the pressure values in the trailing-edge region. If, on the average, the flow is attached most of the time, the mean pressure distributions will indicate that the flow is attached. The mean data give an accurate indication of separation only when the flow remains separated most of the time. Another point to note is that while the wool tufts indicate flow separation, they are inadequate for indicating the subsequent flow reattachment.

Figure 13 shows a time history of upper and lower surface pressures at the same span station and flow conditions as given in Fig. 12. All pressures are arbitrarily plotted so that they fit near each other. However, the last chordwise pressures on both surfaces are plotted with a zero reference line. For the last chordwise pressures the figure clearly shows the separa-

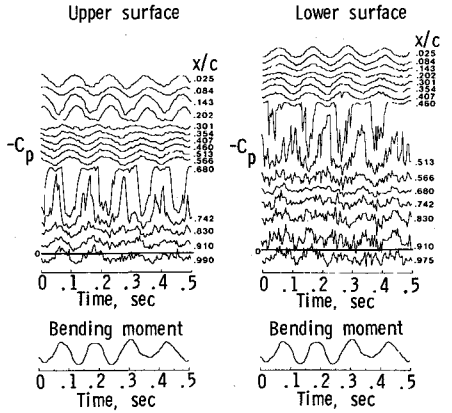

Fig. 13 Pressure variation with time at $\eta = 0.871$, $M = 0.92$, $\alpha = -1$ deg, and $\delta_m = 0$ deg.

tion and reattachment of flow in the trailing-edge region of both surfaces as the pressure values fluctuate above and below zero. The shock motion, as indicated by large pressure variations is also shown in the figure. For example, the upper surface shock can be seen to move from in front of 68.0% of local chord to behind 74.2%. The lower surface shock moves from in front of 46.0% to behind 51.3%. At the bottom of the figure, the measured wing-root bending-moment time history is plotted for reference. For the observed motion, the wing-root bending moment is proportional to wing-tip displacement, being maximum for maxium positive (up) wing-tip position.

Concluding Remarks

Unsteady aerodynamic and response data were measured on a 10.3 aspect-ratio elastic supercritical wing undergoing high dynamic response above Mach number of 0.90. The wing had been tested previously in the NASA Langley TDT, and an unusual instability boundary was predicted based upon subcritical response data. Contrary to the predictions, no instability was found during the present test. Instead, a region of high dynamic wing response was observed, which reached a maximum value between Mach numbers 0.92 and 0.93. The amplitude of the dynamic response increased directly with dynamic pressure. Maximum wing-tip motion observed was 6 in. peak-to-peak. The dynamic wing response was sensitive to angle of attack, with maximum motion occurring near $\alpha = 0$ deg. Static deflection of the outboard control surface was found to decrease significantly the dynamic response for $\delta_m = -6$ deg. A spanwise fence installed on the lower surface at approximately 60% local chordline to disturb the flow pattern resulted in a significant decrease in dynamic wing response.

The response appears to be related to chordwise shock movement in conjunction with flow separation and reattachment on the upper and lower wing surfaces. At Mach numbers above 0.93, the dynamic response rapidly decreases with increasing Mach number. This is likely due to the flow remaining completely separated aft of the shock. Mean pressure data indicate separation only after the flow has become fully separated. Tufts on the wing indicated the onset of flow separation at slightly lower Mach numbers than indicated by the mean pressure data. The onset of flow separation coincided with the occurrence of strong shocks on a surface. Instantaneous pressure distributions indicated that the flow was intermittently separating and reattaching near the trailing edge under conditions of maximum wing motion.

References

[1]Erickson, L. L., "Transonic Single-Mode Flutter and Buffet of a Low-Aspect-Ratio Wing Having a Subsonic Airfoil Shape," NASA TN D-7346, Jan. 1974.

[2]Dobbs, S. K., Miller, G. D., and Stevenson, J. R., "Self-Induced Oscillation Wind-Tunnel Test of a Variable Sweep Wing," AIAA Paper 85-0739, April 1985.

[3]Murrow, H. N. and Eckstrom, C. V., "Drones for Aerodynamic and Structural Testing (DAST)—A Status Report," *Journal of Aircraft*, Vol. 16, Aug. 1979, pp. 521–526.

[4]Seidel, D. A., Sandford, M. C., and Eckstrom, C. V., "Measured Unsteady Transonic Aerodynamic Characteristics of an Elastic Supercritical Wing with an Oscillating Control Surface," *Journal of Aircraft*, Vol. 24, April 1987, pp. 225–230.

[5]Byrdsong, T. A. and Cuyler, W. B., Jr., "Wind-Tunnel Investigation of Longitudinal and Lateral-Directional Stability and Control Characteristics of a 0.237-Scale Model of a Remotely Piloted Research Vehicle With a Thick, High-Aspect-Ratio Supercritical Wing," NASA TM 81790, July 1980.

[6]Eckstrom, C. V., "Loads Calibration of Strain Gage Bridges on the DAST Project Aeroelastic Research Wing (ARW-2)," NASA TM 87677, March 1986.

[7]Cole, P. H., "Wind-Tunnel Real-Time Data Acquisition System," NASA TM 80081, April 1979.

[8]Chapin, W. G., "Dynamic-Pressure Measurements Using an Electronically Scanned Pressure Module," NASA TM 84650, July 1983.

[9]Sandford, M. C., Abel, I., and Gray, D. L., "Development and Demonstration of a Flutter-Suppression System Using Active Controls," NASA TR R-450, Dec. 1975.

[10]Bennett, R. M., Seidel, D. A., and Sandford, M. C., "Transonic Calculations for a Flexible Supercritical Wing and Comparison with Experiment," AIAA Paper 85-0665-CP, April 1985.

[11]Yates, E. C., Jr., Wynne, E. C., and Farmer, M. G., "Effects of Angle of Attack on Transonic Flutter of a Supercritical Wing," *Journal of Aircraft*, Vol. 20, Oct. 1983, pp. 841–847.